# Nanotoxicology

Taylor & Francis
Taylor & Francis Group

ORIGINAL ARTICLE

# Airway irritation, inflammation, and toxicity in mice following inhalation of metal oxide nanoparticles

Søren T. Larsen[1], Petra Jackson[1], Steen S. Poulsen[2], Marcus Levin[1], Keld A. Jensen[1], Håkan Wallin[1], Gunnar D. Nielsen[1], and Ismo K. Koponen[1]

[1]Danish Centre for Nanosafety, National Research Centre for the Working Environment, Copenhagen, Denmark and [2]Department of Biomedical Research, The Panum Institute, University of Copenhagen, Copenhagen, Denmark

## Abstract

Metal oxide nanoparticles are used in a broad range of industrial processes and workers may be exposed to aerosols of the particles both during production and handling. Despite the widespread use of these particles, relatively few studies have been performed to investigate the toxicological effects in the airways following inhalation. In the present study, the acute (24 h) and persistent (13 weeks) effects in the airways after a single exposure to metal oxide nanoparticles were studied using a murine inhalation model. Mice were exposed 60 min to aerosols of either ZnO, TiO$_2$, Al$_2$O$_3$ or CeO$_2$ and the deposited doses in the upper and lower respiratory tracts were calculated. Endpoints were acute airway irritation, pulmonary inflammation based on analyses of bronchoalveolar lavage (BAL) cell composition, DNA damage assessed by the comet assay and pulmonary toxicity assessed by protein level in BAL fluid and histology. All studied particles reduced the tidal volume in a concentration-dependent manner accompanied with an increase in the respiratory rate. In addition, ZnO and TiO$_2$ induced nasal irritation. BAL cell analyses revealed both neutrophilic and lymphocytic inflammation 24-h post-exposure to all particles except TiO$_2$. The ranking of potency regarding induction of acute lung inflammation was Al$_2$O$_3$ = TiO$_2$ < CeO$_2$ ≪ ZnO. Exposure to CeO$_2$ gave rise to a more persistent inflammation; both neutrophilic and lymphocytic inflammation was seen 13 weeks after exposure. As the only particles, ZnO caused a significant toxic effect in the airways while TiO$_2$ gave rise to DNA-strand break as shown by the comet assay.

## Introduction

Metal oxide nanoparticles are important industrial materials and they are used in a broad range of processes and products including paint, catalysts, fuel additives, solar panels, glass polish, sunscreens, cosmetics, and pharmaceutical products. During production of the particles and the later handling by down-stream users, the dry powder can form airborne dust which may be inhaled. Other scenarios for metal oxide particle exposures include aluminum smelting and welding galvanized steel, which liberates Al$_2$O$_3$ and ZnO particles, respectively (Healy et al., 2001; ICRP, 1994).

Various acute health effects after exposure to metal oxides have been observed. Among the best known effect is metal fume fever caused by exposure to ZnO particles. This condition is most commonly seen among welders few hours after welding galvanized steel. Symptoms include chest pain, difficulties in breathing, and flu-like symptoms (Antonini et al., 2003). Apart from zinc, oxides of cadmium, copper, magnesium, and tin may also induce metal fume fever (Antonini et al., 2003). Nickel oxide and chromium oxide, both formed during welding stainless steel, are recognized as lung carcinogens (IARC, 1990) whereas inhalation of copper oxide, magnesium oxide, and barium oxide may give rise to respiratory tract irritation (Antonini et al., 2003).

Pulmonary toxicity of metal oxide nanoparticles has been investigated in animals. Endpoints studied include inflammation, histopathological changes, oxidative stress, and in a few cases also airway irritation. Animals have in most cases been exposed to the material via intratracheal instillation of the material in an aqueous suspension. The vehicle and dispersion protocols vary considerably, making comparison across instillation studies complicated. Furthermore, by bolus instillation, the entire dose is deposited in the lungs within a few seconds, giving rise to an extremely high-dose rate, which may drive a toxic response not seen if the same dose was administered over a longer period (Driscoll et al., 2000). Apart from TiO$_2$, surprisingly few studies of metal oxide toxicity use inhalation of a dry aerosol, although only inhalation reflects real-life exposure.

In inhalation studies, the exposure is often characterized by a mass concentration (e.g. mg/m$^3$) and a particle size distribution. Very few studies estimate the deposited dose in the lungs after airway exposure to a dry aerosol, although this knowledge is crucial in order to compare results from inhalation studies with data from instillation studies.

Correspondence: Søren T. Larsen, Danish Centre for Nanosafety, National Research Centre for the Working Environment, Lersø Parkallé 105, 2100 Copenhagen Ø. Tel: +4539165248. E-mail: stl@nrcwe.dk

In the present study, we exposed mice to one of five different metal oxide nanoparticles by inhalation of a dry aerosol. Investigated effects included acute and subchronic airway inflammation. Furthermore, the pulmonary toxicities of ZnO, TiO$_2$, Al$_2$O$_3$, and CeO$_2$ were assessed based on protein content in bronchoalveolar lavage fluid (BALF) and histological analyses of lung tissue. The levels of DNA-strand breaks, an indicator of genotoxicity, were assessed by the comet assay. Finally, the airway irritation potentials of the inhaled particles were studied, since this provides information related to the ''warning response'' of the particle. Thus, a particle with low airway irritation potential may be inhaled without feeling any discomfort and workers may therefore be unaware of the exposure.

## Methods

### Animals

Inbred female BALB/cJ mice aged 6–7 weeks were purchased from Taconic M&B, Ry, Denmark, and were housed in polypropylene cages ($380 \times 220 \times 150$ mm) with pinewood sawdust bedding (Lignocel S8, Brogaarden, Denmark). The cages were furnished with bedding materials, gnaw sticks, and cardboard tubes. The photo-period was from 6 a.m. to 6 p.m., and the temperature and mean relative humidity in the animal room were 19–22 °C and $43 \pm 8\%$ (SD), respectively. Food (Altromin no. 1324, Altromin, Lage, Germany) and tap water were available *ad libitum*. Treatment of the animals followed procedures approved by The Animal Experiment Inspectorate, Denmark (2011/561-1990). At the time of exposure, the mice had a body weight of $21.1 \pm 2.2$ g (mean $\pm$ SD).

### Chemicals

The following metal oxide nanoparticles were included in the study: two types of ZnO (in the following referred to as ZnO_1 and ZnO_2), TiO$_2$, Al$_2$O$_3$, and CeO$_2$.

The ZnO_2 and CeO$_2$ were from Evonik Degussa, GmbH whereas the ZnO_1, TiO$_2$ and Al$_2$O$_3$ were synthesized by PlasmaChem (Berlin, Germany). The crystal phase of TiO$_2$ was anatase. Other data from the characterization of the particles are given in Table 1. The size and size distribution of the nanoparticles were determined using transmission electron microscopy (TEM), the surface elemental composition was determined by X-ray photoelectron spectroscopy (XPS) and the specific surface areas of the bulk nanoparticles were determined by means of the Brunauer–Emmett–Teller (BET) nitrogen adsorption method as described (Levin et al., 2015).

### Generation of test atmospheres and aerosol characterization

All nanoparticles were aerosolized using a dry powder aerosol generator (Microdosing system, Fraunhofer ITEM, Hannover, Germany). The generator was operated at a pressure of 1.0 bar which generated an airflow of 14.7 L/min. Particle number size distribution spectra of ZnO_1, ZnO_2, TiO$_2$, Al$_2$O$_3$, and CeO$_2$ were characterized using an Electrical Low Pressure Impactor (ELPI+, Dekati Ltd., Kangasala, Finland) which measures the aerodynamic equivalent diameter in 14 channels ranging from 6 nm to 10 μm. The number of distributions was converted to particle mass distributions through assumption of spherical particle shape and unit density. As seen in Table S1 in the Supplementary material, standard deviations of the particle numbers were in general less than 10% during the 1-h exposure. We have used the Fraunhofer microdosing disk method previously and have good experience of it being a stable source for particle delivery. By measuring on-line with ELPI and comparing that data with mass sampled with filter we can verify that our sampled mass concentrations are reliable. Calculations of deposited doses were in all cases based on gravimetrical sampling of particles. Aerosols were continuously collected from the breathing zone of the mice throughout all exposure studied and total aerosol mass concentrations were determined gravimetrically by a filter sampling protocol (Clausen et al., 2003). At higher concentrations, sampling was performed using 2 or 3 filters with a difference in time-weighed mass deposition of less than 25%. The particle size distribution is only to a very little degree affected by the total output of the aerosol generator (cf. Figures in Supplementary material).

Total aerosol mass concentrations in the exposure chamber ranged from 4 to 271 mg/m$^3$ (Table 3). The exposure concentrations were selected based on the toxicological and airway irritation potency of the particles, observed in a pilot scale range finding study. Due to the low inflammogenic and toxic potency of TiO$_2$, this compound was only studied at the highest generable concentration, 271 mg/m$^3$.

### Mouse bioassay

The Notocord Hem (Notocord Systems SA, Croissy-sur-Seine, France) data acquisition software was used to collect and analyze respiratory parameters. Mice were placed in body plethysmographs, which were connected to the exposure chamber, and animals were exposed head-only (Vijayaraghavan et al., 1994). The acquisition program calculates *i.a.* the respiratory rate (f, [breaths per minute]), time from end of inspiration until beginning of the expiration, termed time of break (TB, [s]), tidal volume (VT, [mL]), mid-expiratory flow rate (VD, [mL/s]), and the time of inspiration (TI, [s]). The inspiratory flow rate [mL/s] was calculated as VT/TI. Comprehensive descriptions of the breathing parameters have been made elsewhere (Larsen & Nielsen, 2000; Vijayaraghavan et al., 1994). Data acquisition and calculations were performed as described previously (Larsen et al., 2004).

Following a 5- to 10-min acclimatization period, the mice ($n = 8$–10 per group) were exposed 15 min to laboratory air, in order to obtain control values for each breathing parameter for

Table 1. Characteristics of the studied metal oxide nanoparticles.

| Compound | Primary size[1] (nm) Mean $\pm$ SD | Characteristics[a] | Specific surface area[b] (m$^2$/g) | Density[b] (g/cm$^3$) | Surface elemental composition[b] | Producer |
|---|---|---|---|---|---|---|
| ZnO_1 | $13.2 \pm 5.4$ | Monodisperse, aggregated | 26.2 | 5.6 | 16.9% C, 50.9% O, 32.2% Zn | PlasmaChem |
| ZnO_2 | $36.1 \pm 18.1$ | Polydisperse | 21.9 | 5.6 | 20.7% C, 43.8% O, 35.5% Zn | Degussa-Quimidroga |
| TiO$_2$ | $10.0 \pm 3.6$ | Aggregated | 173.1 | 4.2 | 21.5% C, 42.2% O, 36.3% Ti | PlasmaChem |
| Al$_2$O$_3$ | $13.6 \pm 8.4$ | Polydisperse | 76.3 | 4.0 | 5.5% C, 46.1% O, 48.4% Al | PlasmaChem, Berlin |
| CeO$_2$ | $13.0 \pm 12.1$ | Polydisperse | 56.7 | 7.2 | 22.1% C, 60.8% O, 17.0% Ce | Evonik-Degussa |

[a]Data from Pérez-Campaña et al. (2012, 2013).
[b]Data from Levin et al. (2015)

each mouse. The baseline period was followed by a 60-min exposure period, to allow the study of time-dependent respiratory changes. After end of exposure, the mice were exposed to clean laboratory air for 15 min, termed the recovery period.

Airway irritants may exert their action at different locations of the respiratory tract depending on the pharmacological nature of the compound and the deposition site, which is dependent on physicochemical properties of the compound as well as its the particle size. Based on the respiratory parameters, it is possible to categorize the irritation as *sensory irritation*, *airflow limitation*, or *pulmonary irritation*. Sensory irritation is caused by a direct stimulation of the trigeminal nerve endings in the upper respiratory tract (URT, Alarie, 1973; Nielsen, 1991). This effect decreases the respiratory rate due to an elongation of the TB, which is a specific marker of sensory irritation.

Stimulation of vagal nerve endings at the alveolar level results in characteristic modifications of the breathing pattern. One type of reflex reaction may be rapid, shallow breathing (RSB), which is characterized by a decrease in VT and an increased respiratory rate.

### Estimating the deposited doses

To estimate the inhalable fraction (IF) of the exposed particle concentrations, we used the method presented by Asgharian and coworkers (2003, 2014) and Menache et al. (1995). In this way, IFs were calculated using a semi-empirical equation developed for rats and parametrized for mice by Asgharian et al. (2014).

$$IF = 1 - \frac{1}{1 + \alpha(\rho d_{ae}^2 Q)^\beta}$$

where coefficients for mice are $\alpha = 9.92$ and $\beta = -0.7466$, $\rho$ is particle density, $d_{ae}$ is aerodynamic diameter, and Q is inspiratory flow rate (cf. Table 2). For all particles, a density of 1 g/cm$^3$ was applied.

To calculate the deposition efficiency in the URT the method described by Asgharian et al. (2014) was used. The URT starts from the nasal openings and extended through the nasal passages, pharynx and larynx until the beginning of the trachea (Asgharian et al., 2014). URT deposition was calculated for inertial deposition and deposition by diffusion. URT deposition for estimating inertial impaction ($\eta_{H-imp}$) was calculated using the method first presented by Zhang & Yu (2015)

$$\eta_{H-imp} = \left[ \frac{(d_{ae}^2 Q)^\alpha}{10^5 + (d_{ae}^2 Q)^\alpha} \right]^\beta$$

where coefficients for the mice are $\alpha = 3.96$ and $\beta = 0.117$ (Asgharian et al., 2014).

Deposition efficiency by diffusion ($\eta_{H-diff}$) was calculated using

$$\eta_{H-diff} = 1 - e^{-\alpha D^\beta Q^\gamma}$$

where D is the diffusion coefficient [cm$^2$/s], $\alpha = 13.688$ (inhalation), $\beta = 0.517$, and $\gamma = -0.234$ (Asgharian et al., 2014), coefficients $\alpha$, $\beta$, and $\gamma$ were derived by Cheng et al. (1990).

Following the method presented by Asgharian et al. (2014), the inhaled fraction was calculated for the lower respiratory tract (LRT). The LRT includes the conducting airways (tracheo-bronchial (TB) region) and the pulmonary region (PUL) (cf. Table 3). The TB comprises the trachea, bronchi, and bronchioles whereas PUL is the alveolar ducts and sacs. Taken together, the LRT comprises 22 airway generations (Asgharian et al., 2014).

Table 2. Respiratory parameters.

| Material | Total concentration (mg/m$^3$) | Breathing frequency (min$^{-1}$) 0–60 min | Tidal volume (µL) 0–60 min | Inspiratory flow rate (mL/s) 0–60 min |
|---|---|---|---|---|
| Control | 0 | $254 \pm 7$ | $193 \pm 18$ | 1.69 |
| ZnO_1 | 6 | $234 \pm 21$ | $184 \pm 22$ | 1.63 |
| | 58 | $210 \pm 16$ | $162 \pm 20$ | 1.42 |
| | 203 | $185 \pm 10$ | $116 \pm 16$ | 1.03 |
| ZnO_2 | 4 | $257 \pm 10$ | $226 \pm 19$ | 2.07 |
| | 26 | $244 \pm 20$ | $221 \pm 10$ | 2.13 |
| | 53 | $224 \pm 21$ | $214 \pm 24$ | 1.89 |
| TiO$_2$ | 271 | $198 \pm 9$ | $170 \pm 22$ | 1.49 |
| Al$_2$O$_3$ | 23 | $256 \pm 6$ | $148 \pm 23$ | 1.35 |
| | 94 | $295 \pm 14$ | $137 \pm 16$ | 1.26 |
| | 235 | $330 \pm 15$ | $137 \pm 14$ | 1.25 |
| CeO$_2$ | 8 | $248 \pm 17$ | $180 \pm 17$ | 1.62 |
| | 30 | $277 \pm 19$ | $160 \pm 15$ | 1.42 |
| | 152 | $314 \pm 17$ | $138 \pm 13$ | 1.24 |

Values are mean $\pm$ SD.

Table 3. Exposure concentrations and estimated deposited doses.

| Material | Total concentration (mg/m$^3$) | Inhaled volume over 60 min (L) | Estimated deposited dose (µg) | | | |
|---|---|---|---|---|---|---|
| | | | LRT | | | |
| | | | PUL | TB | URT | Total deposited in airways |
| ZnO_1 | 6 | 2.594 | 0.04 | 0.14 | 2.12 | 2.30 |
| | 58 | 2.024 | 0.41 | 1.37 | 20.6 | 22.3 |
| | 203 | 1.296 | 1.45 | 4.79 | 72.1 | 78.1 |
| ZnO_2 | 4 | 3.489 | 0.02 | 0.09 | 1.28 | 1.31 |
| | 26 | 3.236 | 0.14 | 0.55 | 8.29 | 8.49 |
| | 53 | 2.874 | 0.19 | 0.64 | 16.9 | 17.0 |
| TiO$_2$ | 271 | 2.021 | 0.60 | 1.50 | 88.7 | 90.5 |
| Al$_2$O$_3$ | 23 | 2.275 | 0.13 | 0.41 | 8.00 | 8.82 |
| | 94 | 2.423 | 0.55 | 1.69 | 32.7 | 36.0 |
| | 235 | 2.709 | 1.21 | 3.81 | 80.2 | 86.6 |
| CeO$_2$ | 8 | 2.683 | 0.06 | 0.17 | 2.77 | 3.13 |
| | 30 | 2.672 | 0.21 | 0.65 | 10.4 | 11.8 |
| | 152 | 2.598 | 0.76 | 2.38 | 51.3 | 54.3 |

The upper respiratory tract (URT) starts at the nasal openings and ends at the beginning of the trachea. The lower respiratory tract (LRT) includes 22 airway generations and can be divided into the tracheo-bronchial (TB, trachea, bronchi, and bronchioles) region and the pulmonary (PUL, alveolar ducts, and sacs) region.

Deposition fractions were calculated applying the ICRP model (Hinds, 1999; ICRP, 1994). Total deposition fraction (DFtot) is the sum of URT, TB, and PUL deposition fractions (cf. Figure 1).

The deposited dose was calculated using the following equation:

$$\text{Deposited dose} = f \times VT \times t \times c \times df,$$

where $f$ = respiratory frequency [breath/minute], $VT$ = tidal volume [mL/breath], $t$ = exposure time [minutes], $c$ = concentration of particle in the size fraction [ng/mL = mg/m$^3$], $df$ = deposited fraction.

The LRT-deposited dose was applied for assessing the inflammatory and toxic properties of the particles. Since the airway irritation response of the particles is driven by the concentration (deposited dose pr. time unit) rather than total
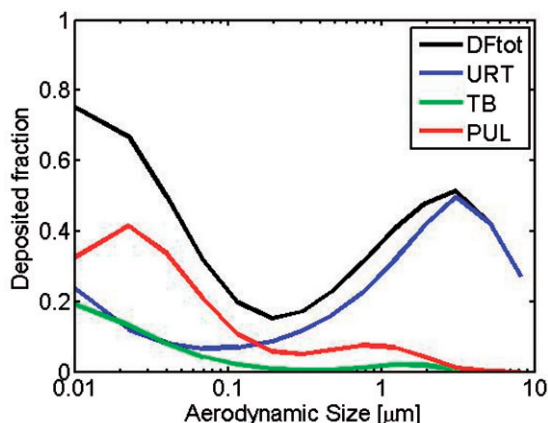


Figure 1. Regional deposition fractions in mice lung of inhaled particles via nasal breathing. Upper respiratory tract (URT): from nasal openings to the beginning of the trachea. Tracheo-bronchial region (TB): trachea, bronchi and bronchioles. Pulmonary region (PUL): alveolar ducts and sacs. DFtot = URT + TB + PUL.

deposited dose, we also apply the unit ''deposited dose per hour'' in these cases (Figure 2b and c). Furthermore, as another important aim of this study was to calculate from total air concentration to actual deposited doses in different regions of the airways, we also present the total air concentration (mg/m$^3$), e.g. Table 3.

## Bronchoalveolar lavage procedure

The study of BAL cell composition was used to assess lung inflammation. BAL cells were recovered by flushing the lungs four times with 0.8 mL of physiological saline using a tracheal cannula. The BAL fluids recovered were pooled and centrifuged (500 g, 10 min, 4 °C). The supernatant was stored for later analyses and the pellet was re-suspended in a 100 μL PBS buffer containing heparin (20 IE/mL) and serum albumin (0.003%). The total numbers of cells were determined using a hemocytometer. For differential counts, cytospin preparations were made (Cytospin®2, StatSpin® Inc., Norwood, MA) (1000 g, 4 min, RT). Slides were stained with May-Grünwald/Giemsa and all slides were inspected in a blinded manner by the same technician. Cells were identified by standard morphology and differentiated into neutrophils, eosinophils, epithelial cells, lymphocytes, and macrophages. For each slide, 200 cells were counted.

## Assessment of genotoxicity

DNA-strand break levels were analyzed by the comet assay described previously by Jackson et al. (2013). The strand breaks measured by the assay present a mixture of different strand breaks, alkaline labile sites, and transient breaks in the DNA due to repair process (Collins, 2009). DNA-strand breaks were determined on frozen BAL cell suspensions and lung tissue. Organ samples were snap frozen in cryotubes (NUNC, Roskilde, Denmark) directly after dissection and kept at −80 °C until analysis. Sample preparation and analysis was previously described in detail (Jackson et al., 2013). BAL cells preserved
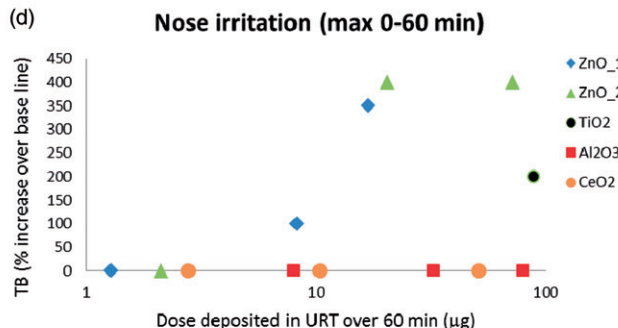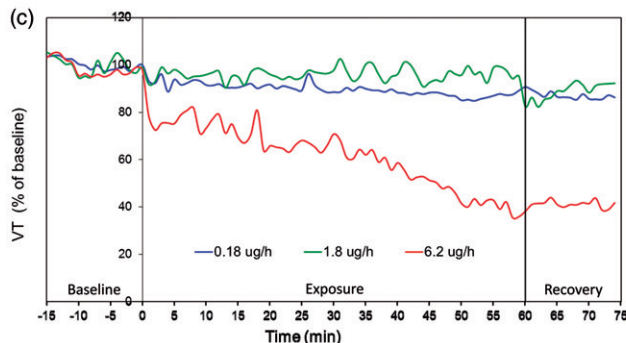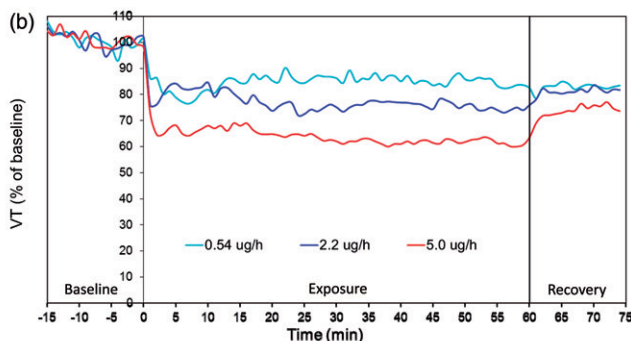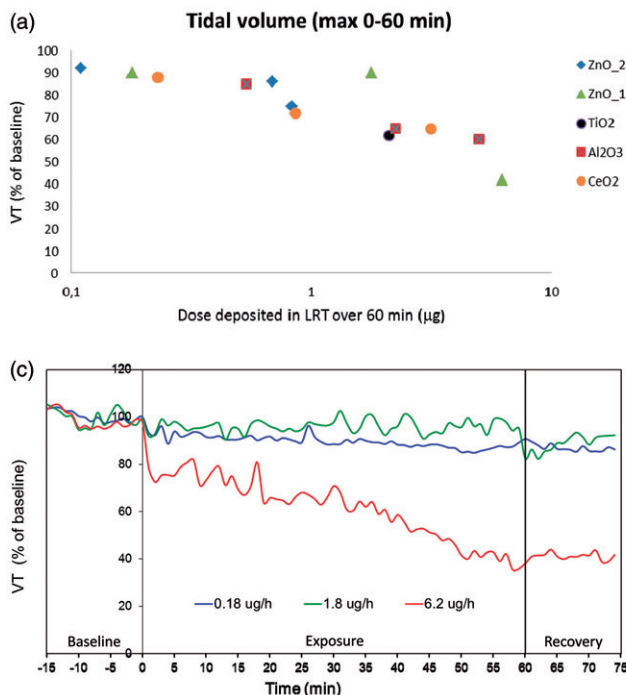


Figure 2. Effects of metal oxide nanoparticle exposures on selected breathing parameters. The tidal volume (VT) values are expressed as minimum average values of 8–10 mice during the 60-min exposure period (a) or as time-response relationship for Al$_2$O$_3$ nanoparticles (b) or ZnO_1 (c). Figure 2d shows the degree of nose irritation quantified by the time of break (TB) elongation.

in dimethyl sulfoxide were thawed quickly at 37 °C, while frozen tissues were homogenized in Merchant's medium. Cells were suspended in agarose at 37 °C, with final agarose concentration of 0.7%. Cells were embedded on Trevigen CometSlides™ (30 μL per well for 20 well slide). Cooled slides were placed in lysis buffer overnight at 4 °C. Next day, slides were rinsed in electrophoresis buffer, alkaline treated for 40 min. Electrophoresis was run with 5% circulation (70 mL/min) for 20 or 30 min (BAL and lung, respectively) at applied voltage 1.15 V/cm (38 V measured for whole electrophoresis chamber) and measured current 300 mA. Slides were neutralized twice for 5 min, fixed in ethanol for 5 min and on warm plate at 45 °C for 15 min. Cells were stained in 20 mL/slide bath with TE buffered SYBR®Green fluorescent stain for 15 min, dried at 37 °C for 10 min, UV-filter and cover slip were applied and DNA damage was analyzed by IMSTAR Pathfinder™ system. Related samples were placed in same electrophoresis. The results are presented as average % DNA in tail and tail length value for all cells scored on each Trevigen CometSlides™ well (average cells counted ± SD; BAL: $885 \pm 375$, lung: $1322 \pm 611$). The day-to-day variation and electrophoresis efficiency was validated by including on each slide A549 epithelial lung cells exposed to PBS or 60 μM $H_2O_2$, used as our negative and positive historical controls for the electrophoresis (Jackson et al., 2013). The day-to-day variation including all slides (n = 16, 8 for each electrophoresis) from this experiment was 24 and 18%, BAL and lung, respectively.

### Protein in BAL fluid

Total protein in BALF was determined using the BCA Protein Assay Kit from Pierce, Rockford, IL according to the manufacturer's instructions.

### Histology

After collection of BALF, the lungs were fixed in situ. The chests of the mice were opened and a polyethylene tube introduced into the trachea. The polyethylene tube was connected to a syringe containing 4% buffered paraformaldehyde, and the lungs were inflated with the fixative to normal size. After 5 min, the lungs were removed in toto and further fixated in formalin for at least 24 h. Tissues were embedded in paraffin in a standardized way (horizontal cut through the hilum regions) and subsequently 7 μm thick slices were cut and stained with periodic acid-Schiff (PAS) hematoxylin and examined for inflammation and morphological changes by conventional bright field microscopy.

### Statistics

The following test procedure was applied in order to reduce the number of pair-wise comparisons: First, the numbers of inflammatory cells in BAL fluid in the exposure groups were compared to the air control group by the Kruskall–Wallis non-parametric ANOVA test. Only if a statistically significant effect was apparent, the individual exposure groups were further compared to the air group by Mann–Whitney's *U* test. A p value of 0.05 or less was considered statistically significant. The same procedure was applied for the protein concentration in BAL fluid and the data from the comet assay. Calculations were performed using the Minitab Statistical Software, Release 14 Xtra (Minitab Inc., State College, PA).

### Results

### Generation and characterization of aerosols

Measurements of all materials were showing similar number distributions, number size distribution spectra were peaking from

295 ($Al_2O_3$) nm to 504 nm $TiO_2$ and modal number concentrations from $1.3e4 \, cm^{-3}$ ($ZnO\_2$) to $2.4e6 \, cm^{-3}$ ($Al_2O_3$). Detailed information on the particle sizes and concentrations is presented in the Supplementary material. Particle size distributions were largely independent on the particle concentration. The calculated mass size distribution spectra were peaking in around 1 μm. Table 1 presents a primary size of these materials and it is apparent that particles in the aerosol are aggregates or agglomerates of primary particles.

### Particle deposition in the airways

Based on particle size distribution of the aerosol, the particle concentration, minute ventilation, and inspiratory flow rate (cf. Method section), estimates of the deposited doses were calculated (Tables 2 and 3). Total deposited doses (URT + LRT) ranged from 1.31 to 90.5 μg per animal during the 60-min exposure period. In all cases, the major part of the dose was deposited in the URT, whereas 0.11–6.24 μg reached the LRT. Only minor doses (0.02–1.45 μg) reached the PUL.

### Airway irritation

All particles studied induced a time- and concentration-dependent reduction in the tidal volume (Figure 2a–c). No major difference was seen in maximum suppression of the tidal volume among the particles (Figure 2a). However, the kinetics of the responses were different; for $TiO_2$, $Al_2O_3$, and $CeO_2$ and the response was characterized by a rapid onset of effect reaching full response after a few minutes of exposure, followed by a plateau throughout the exposure period. After cessation of exposure, the response partly returned to baseline level. As an example, the response to $Al_2O_3$ is shown in Figure 2(b). For $Al_2O_3$ and $CeO_2$, the reduction in tidal volume was accompanied by an increase in respiratory frequency (Table 2). The two types of ZnO particles gave rise to another type of response; for these particles, a gradual reduction in tidal volume was observed during the whole 60-min exposure period. During the 15-min post-exposure period, no recovery of the mice was observed. As an example, the response for $ZnO\_1$ is shown in Figure 2(c). Follow-up measurement 6- and 24 h after exposure showed little normalization of the breathing (data not shown). For all studied particles, the decrease in tidal volume was accompanied by a reduction in the expiratory flow rate (data not shown).

Another type of airway effects, sensory (nose) irritation, was observed after exposure to $TiO_2$ and both types of ZnO. Sensory irritation response can be identified and quantified from the elongation of the TB (Figure 2d). Neither $Al_2O_3$ nor $CeO_2$ induced any nose irritation even at the highest exposure concentrations (Figure 2d). The elongated TB in the $TiO_2$ and the two ZnO groups reduced the breathing frequency in these animals (Table 2).

### Lung inflammation

Exposure to $ZnO\_1$ as well as $ZnO\_2$ gave rise to an increased number of both neutrophils (Figure 3a) and lymphocytes (Figure 3b) in the BAL fluid 24-h post-exposure. In contrast, neither $TiO_2$ nor $Al_2O_3$ exposure gave rise to any significant increase in the number of inflammatory cells even at the highest doses deposited in the LRT (2.1 and 5.0 μg, respectively).

The potency of the particles to induce acute neutrophilic lung inflammation was: $Al_2O_3 = TiO_2 < CeO_2 < ZnO\_1 < ZnO\_2$.

Based on lymphocytic inflammation, the ranking was $Al_2O_3 = TiO_2 = CeO_2 < ZnO\_1 < ZnO\_2$.

In general, the studied particles had little effect on the number of alveolar macrophages in BAL fluid (Figure 3c). However,

(a)

**Neutrophils 24 h post exposure**



(b)

**Lymphocytes 24 h post exposure**



(c)

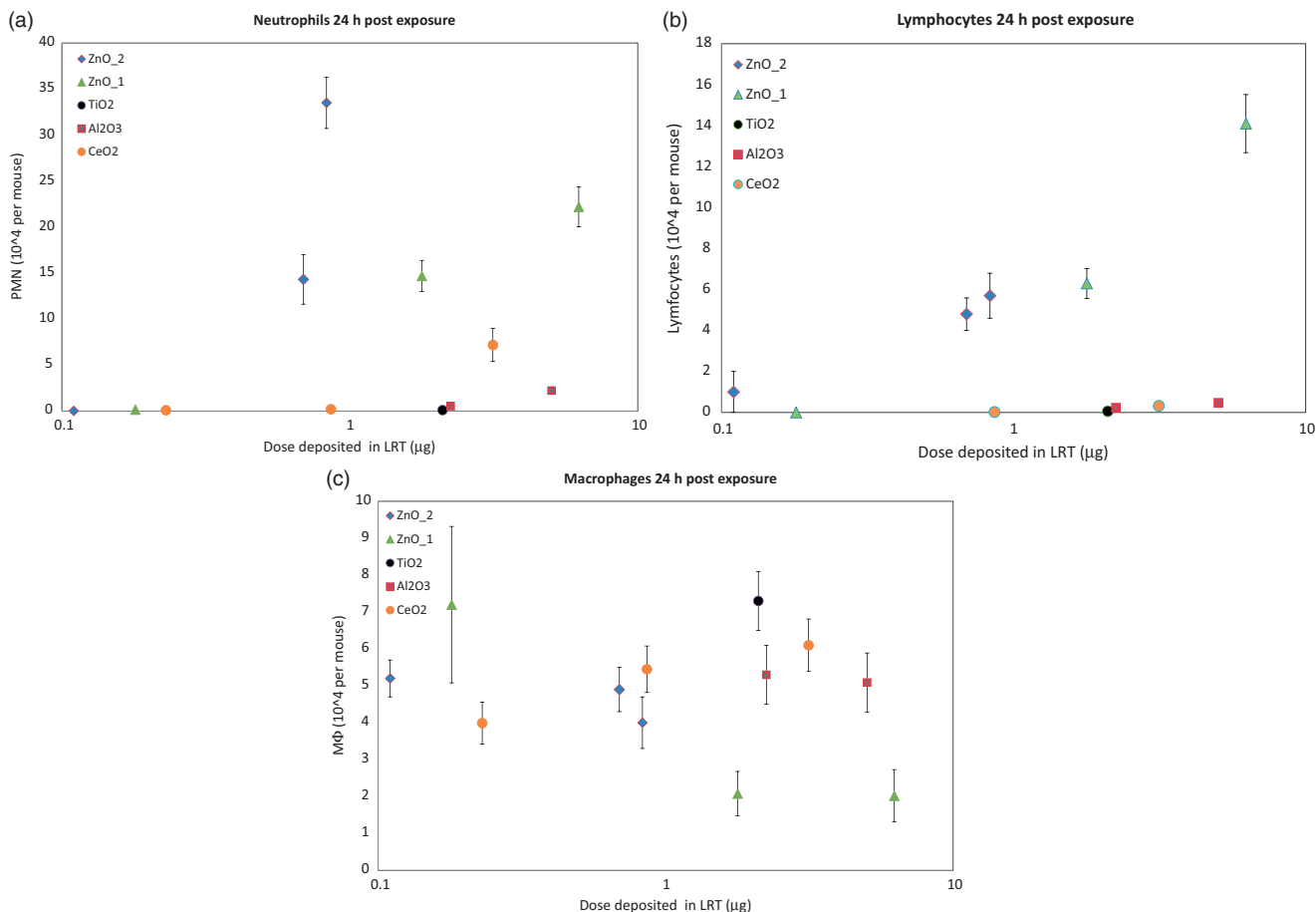**Macrophages 24 h post exposure**



Figure 3. Neutrophils (a), lymphocytes (b) and macrophages (c) in BAL fluid from mice 24 h after exposure to metal oxide nanoparticle giving rise to lower respiratory depositions of 0.11–6.2 μg. Mean ± SEM of groups of 8–10 mice are presented.

exposure to ZnO_1 caused a reduction in the macrophage number ($p < 0.05$). The other ZnO particle studied, ZnO_2, did not induce a similar effect.

13 weeks after exposure, increased levels of both neutrophils and lymphocytes were only seen in mice exposed to $CeO_2$ (data not shown).

### Genotoxicity

One-hour exposure to $TiO_2$ resulting in a LRT deposition of 2.1 μg increased levels of DNA-strand breaks in the lung tissue detectable 24 h after exposure. DNA-strand breaks shown by the comet assay were apparent both from tail length and % DNA in the tail (Table 4). The other investigated particles did not increase DNA-strand breaks significantly.

### Lung toxicity

Toxic effect of inhaled particles was seen for both types of ZnO, where increased levels of total protein were seen in BALF 24-h post-exposure (Table 4). The ZnO_2 appears to be more toxic than the ZnO_1 since 26 mg/m³ ZnO_2 (0.69 μg deposited in LRT) gave rise to a protein level in BAL equivalent to 58 and 203 mg/m³ ZnO_1 (corresponding to 1.78 and 6.24 μg deposited in LRT).

No increased protein levels in BALF were observed 13 weeks after exposure (data not shown).

The toxic effect of 53 mg/m³ ZnO_2 (0.83 μg deposited in LRT) on the lung tissue was further confirmed by histology. Desquamation of bronchiolar cells (Figure 4b) and vacuolization and necrosis of Clara cells (Figure 4c) was seen in the mice 24 h

Table 4. Toxicological effects of metal oxide nanoparticle exposure.

| Material | Particle concentration (mg/m³) | Protein in BAL fluid (μg/mL) | Comet assay | |
|---|---|---|---|---|
| | | | Tail length | % DNA in tail |
| Control | 0 | 146 ± 51 | 21.2 ± 2.6 | 6.0 ± 0.8 |
| ZnO_1 | 6 | 94 ± 22 | – | – |
| | 58 | 399 ± 70*** | 27.5 ± 4.6 | 9.9 ± 2.5 |
| | 203 | 371 ± 195** | – | – |
| ZnO_2 | 4 | 204 ± 102 | 33.3 ± 8 | 10.6 ± 3.3 |
| | 26 | 422 ± 179*** | 27.3 ± 6.4 | 8.8 ± 1.7 |
| | 53 | 655 ± 285*** | 23.7 ± 2.9 | 14.2 ± 13.1 |
| TiO₂ | 271 | 234 ± 145 | 39.0 ± 9.5* | 20 ± 8.6* |
| Al₂O₃ | 23 | – | 22.6 ± 1.9 | 7.4 ± 1.6 |
| | 94 | 303 ± 134 | 23.4 ± 4.9 | 8.0 ± 2.7 |
| | 235 | 213 ± 51 | 32.2 ± 7.4 | 11.4 ± 4.8 |
| CeO₂ | 8 | 116 ± 86 | 36.5 ± 9.2 | 19.3 ± 8.5 |
| | 30 | 107 ± 71 | 23.1 ± 5.8 | 7.2 ± 2.5 |
| | 152 | 149 ± 65 | 28.4 ± 9.5 | 11.7 ± 6.7 |

Values are mean ± SD. Statistically significant increases compared to the negative control group are indicated by *$p \leq 0.05$, **$p \leq 0.01$, or ***$p \leq 0.001$.

after ZnO_2 exposure. No histological change was seen 13-week post-exposure in any of the exposure groups.

### Discussion

In the present study, we investigated the inflammogenic and toxic properties of a range of metal oxide nanoparticles. Of the studied
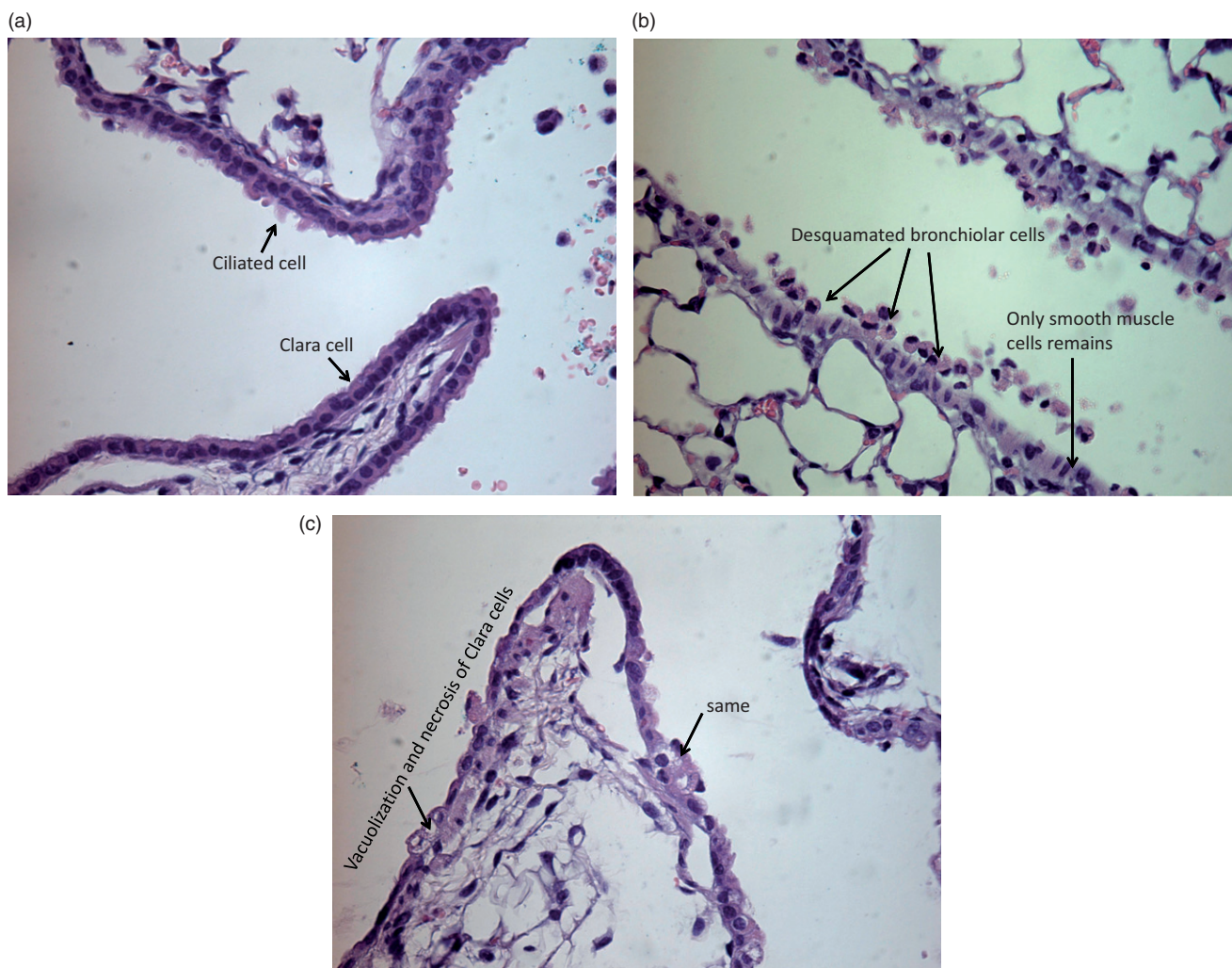
Figure 4. Lung from mouse 24 h after exposure to air (a) or ZnO_2 (b and c). ZnO exposure lead to desquamation of bronchiolar cells as shown in panel b, and vacuolization and necrosis of Clara cells (c). The deposited dose of Zn_2 in the lower respiratory tract is 0.83 μg. The slide section is representative for effects seen in the group.

particles, the two types of ZnO were by far the most inflammogenic. ZnO was also the most toxic substance assessed by protein content in BALF and by histological analyses. Inflammation as well as toxic effect occurred after 1-h exposure to 26 mg/m$^3$ ZnO_2 and 58 mg/m$^3$ ZnO_1 corresponding to LRT deposited doses of 0.69 and 1.78 μg per mouse, respectively (approx. 30 and 80 μg/kg, respectively) (cf. Table 3). This observation is in line with another inhalation study, where rats were exposed 6 h to ZnO nanoparticles with a diameter of 35 or 250 nm, respectively. Lung inflammation and increased BALF protein was seen at concentrations of 12.1 and 45.2 mg/m$^3$, for the 35 nm and 250 nm particle sizes, respectively (Ho et al., 2011). Chen et al. (2015) exposed mice to 0.86 mg/m$^3$ ZnO nanoparticles for 5 h. The primary particle size was about 9 nm whereas the particle aggregates/agglomerates in the aerosol was about 67 nm in average. Acute lung inflammation, mainly located at the bronchoalveolar junctions, was seen 24-h post-exposure. Inflammatory effect of ZnO has also been demonstrated in rodents after intratracheal instillation, although at much higher doses. Thus Sayes et al. (2007) instilled 1 or 5 mg/kg of ZnO nanoparticles or fine ZnO particles intratracheally in rats. Twenty-four hours after exposure, lung inflammation, based on total cell number in BALF, was absent at the 1 mg/kg level, whereas 5 mg/kg nanosized (but not microsized) particles induced inflammation. This is in line with observations recently reported by Jacobsen et al. (2015), where both neutrophilic as well as lymphocytic inflammation was absent 1 day after instillation or aspiration of 18 μg ZnO/mouse, corresponding to approx. 1 mg/kg. In the study by Jacobsen et al. (2015), no increased protein level in BALF was observed 24 h after instillation of doses up to 18 μg/mouse. In the present inhalation study, statistically significant increased levels of lavageable protein were seen after LRT deposition of only 0.7 μg ZnO per mouse. This suggests that inhalation studies may be more sensitive than instillation studies to reveal adverse effects of particles.

The low inflammatory potency of TiO$_2$ seen in the present study is supported by previous studies where TiO$_2$ particles were administered by inhalation (Leppanen et al., 2015) or instillation (Warheit et al., 2006, 2007). Cho et al. investigated the inflammatory effects of several metal oxide nanoparticles (Cho et al., 2012). Rats were i.t. instilled with two different doses of particles and endpoints were evaluated 24-h and 4-week post-exposure, respectively. Based on BAL fluid cells, CeO$_2$ and ZnO were both able to induce inflammation 24 h after instillation, whereas no inflammatory effects were seen by TiO$_2$, which is fully in accordance with our observations. Cho et al. (2012) showed that 4 weeks after instillation of CeO$_2$, increased levels of neutrophils were seen, which is also in agreement with observations in the present study.

The DNA-damaging effect of TiO$_2$ observed in the present study is in line with other studies exposing different cell types to nanosized TiO$_2$ (Gopalan et al., 2009; Karlsson et al., 2008;

Wang et al., 2007). In a study comparing the DNA-damaging potency of a range of different metal oxide nanoparticles, including CuO, $TiO_2$, ZnO, and iron oxides, $TiO_2$ was found to be more potent than ZnO (Karlsson et al., 2008). This result is also confirmed in the present study.

The airway irritation potential of metal oxide nanoparticles has only been assessed for a limited number of substances. Recently, $TiO_2$ was studied (Leppanen et al., 2011, 2015). It was found that $TiO_2$ nanoparticles with a primary particle size of approx. 20 nm and a peak in aggregate size of about 100 nm gave rise to airway effects at a concentration of 8 mg/m$^3$. The main effect was a reduced expiratory flow rate and a minor sensory irritation. Exposure to larger, pigment grade $TiO_2$ particles induced only minor respiratory effects, suggesting that particle size may play a role for sensory irritation response. In the present study, both ZnO and $TiO_2$ induced sensory irritation, the first being the more potent. The $TiO_2$ particle we used was stabilized with nitric acid, and a part of the sensory irritation response may therefore be due to residues of acid, which is a strong airway irritant. The airway irritation of ZnO may be driven by a direct stimulation of the transient receptor ankyrin (TRP) A1 receptor since previous study has shown that the $Zn^{2+}$ ion is a specific agonist for this receptor (Hu et al., 2009).

Whereas the sensory irritation response is most likely due to activation of specific receptors, all studied particles, irrespective of chemical composition, reduced the tidal volume in a concentration-dependent manner. No difference in potency was seen across the particles, suggesting that the onset of this type of airway response may be due to a nonspecific physical reaction. However, whereas the effects rapidly resolved after cessation of exposure for $TiO_2$, $Al_2O_3$, and $CeO_2$ the two types of ZnO induced a more persistent response which did not resolve within 24 h, suggesting that the airway response of ZnO includes another mechanism. One possible explanation is that the more persistent depression may be driven by the toxic effects of ZnO. Exposure to ZnO increased the level of proteins in the lungs due to extravasation of blood protein. Albumin, the most abundant protein in the blood, is a well-known and potent inhibitor of lung surfactants (LS) (Taeusch et al., 2005). The function of LS is to reduce the surface tension at the air–liquid interface in the bronchioles and alveoli thereby making breathing more effortless. The high levels of protein in BAL fluid from ZnO-exposed mice are therefore likely to contribute to the pronounced and long-lasting depression of the tidal volume through LS inactivation by albumin. LS inhibition has shown to lead to partial alveolar collapse (Taeusch et al., 2005) which consequently reduces the tidal volume as observed in the present study. The toxicity of ZnO in the lungs has previously been proposed to be mediated by $Zn^{2+}$ ions (Cho et al., 2011). However, the dissolution of ZnO mainly takes place in the cytosol of macrophages and the rapid onset of pulmonary effects (<60 min of exposure) suggest a direct effect of the ZnO particles *per se*. Furthermore, particles may directly interact with the LS film, which may impair the LS function making breathing labored. It could be speculated that inhaling low-soluble particles may compromise LS function due to adsorption of LS components such as phospholipids or LS-associated proteins as previously shown for nanosized $TiO_2$ particles (Schleh & Hohlfeld, 2009).

## Acknowledgements

## Declaration of interest

The authors report no conflicts of interest. The authors alone are responsible for the content and writing of this article.

## References

Alarie Y. 1973. Sensory irritation by airborne chemicals. CRC Crit Rev Toxicol 2:299–363.

Antonini JM, Lewis AB, Roberts JR, Whaley DA. 2003. Pulmonary effects of welding fumes: review of worker and experimental animal studies. Am J Ind Med 43:350–60.

Asgharian B, Kelly JT, Tewksbury EW. 2003. Respiratory deposition and inhalability of monodisperse aerosols in Long-Evans rats. Toxicol Sci 71:104–11.

Asgharian B, Price OT, Oldham M, Chen LC, Saunders EL, Gordon T, et al. 2014. Computational modeling of nanoscale and microscale particle deposition, retention and dosimetry in the mouse respiratory tract. Inhal Toxicol 26:829–42.

Chen JK, Ho CC, Chang H, Lin JF, Chung SY, Tsai MH, et al. 2015. Particulate nature of inhaled zinc oxide nanoparticles determines systemic effects and mechanisms of pulmonary inflammation in mice. Nanotoxicology 9:43–53.

Cheng YS, Hansen GK, Su YF, Yeh HC, Morgan KT. 1990. Deposition of ultrafine aerosols in rat nasal molds. Toxicol Appl Pharmacol 106: 222–33.

Cho WS, Duffin R, Howie SE, Scotton CJ, Wallace WA, Macnee W, et al. 2011. Progressive severe lung injury by zinc oxide nanoparticles: the role of $Zn^{2+}$ dissolution inside lysosomes. Part Fibre Toxicol 8:27.

Cho WS, Duffin R, Thielbeer F, Bradley M, Megson IL, Macnee W, et al. 2012. Zeta potential and solubility to toxic ions as mechanisms of lung inflammation caused by metal/metal oxide nanoparticles. Toxicol Sci 126:469–77.

Clausen SK, Bergqvist M, Poulsen LK, Poulsen OM, Nielsen GD. 2003. Development of sensitisation or tolerance following repeated OVA inhalation in BALB/cJ mice. Dose-dependency and modulation by the $Al(OH)_3$ adjuvant. Toxicology 184:51–68.

Collins AR. 2009. Investigating oxidative DNA damage and its repair using the comet assay. Mutat Res 681:24–32.

Driscoll KE, Costa DL, Hatch G, Henderson R, Oberdorster G, Salem H, Schlesinger RB. 2000. Intratracheal instillation as an exposure technique for the evaluation of respiratory tract toxicity: uses and limitations. Toxicol Sci 55:24–35.

Gopalan RC, Osman IF, Amani A, De Matas M, Anderson D. 2009. The effect of zinc oxide and titanium dioxide nanoparticles in the Comet assay with UVA photoactivation of human sperm and lymphocytes. Nanotoxicology 3:33–9.

Healy J, Bradley SD, Northage C, Scobbie E. 2001. Inhalation exposure in secondary aluminium smelting. Ann Occup Hyg 45:217–25.

Hinds WC. 1999. Technology, Properties, Behavior and Measurements of Airborne Particles. 2nd ed. New York: Wiley.

Ho M, Wu KY, Chein HM, Chen LC, Cheng TJ. 2011. Pulmonary toxicity of inhaled nanoscale and fine zinc oxide particles: mass and surface area as an exposure metric. Inhal Toxicol 23:947–56.

Hu H, Bandell M, Petrus MJ, Zhu MX, Patapoutian A. 2009. Zinc activates damage-sensing TRPA1 ion channels. Nat Chem Biol 5: 183–90.

IARC. 1990. Chromium, Nickel and Welding. International Agency for Research on Cancer. IARC Monographs on the evaluation of carcinogenic risks to humans [49].

ICRP. 1994. Human respiratory tract model for radiological protection. Ann ICRP 24:1–3. ICRP publication 66.

Jackson P, Pedersen LM, Kyjovska ZO, Jacobsen NR, Saber AT, Hougaard KS, et al. 2013. Validation of freezing tissues and cells for analysis of DNA strand break levels by comet assay. Mutagenesis 28: 699–707.

Jacobsen NR, Stoeger T, van den Brule S, Saber AT, Beyerle A, Vietti G, et al. 2015. Acute and subacute pulmonary toxicity and mortality in mice after intratracheal instillation of ZnO nanoparticles in three laboratories. Food Chem Toxicol 85:84–95.

Karlsson HL, Cronholm P, Gustafsson J, Möller L. 2008. Copper oxide nanoparticles are highly toxic: a comparison between metal oxide nanoparticles and carbon nanotubes. Chem Res Toxicol 21: 1726–32.

Larsen ST, Hansen JS, Hammer M, Alarie Y, Nielsen GD. 2004. Effects of mono-2-ethylhexyl phthalate on the respiratory tract in BALB/c mice. Hum Exp Toxicol 23:537–45.

Larsen ST, Nielsen GD. 2000. Effects of methacrolein on the respiratory tract in mice. Toxicol Lett 114:197–202.

Leppanen M, Korpi A, Miettinen M, Leskinen J, Torvela T, Rossi EM, et al. 2011. Nanosized $TiO_2$ caused minor airflow limitation in the murine airways. Arch Toxicol 85:827–39.

Leppanen M, Korpi A, Yli-Pirila P, Lehto M, Wolff H, Kosma VM, et al. 2015. Negligible respiratory irritation and inflammation potency of pigmentary $TiO_2$ in mice. Inhal Toxicol 27:378–86.

Levin M, Rojas E, Vanhala E, Vippola M, Liguori B, Kling KI, et al. 2015. Influence of relative humidity and physical load during storage on dustiness of inorganic nanomaterials: implications for testing and risk assessment. J Nanopart Res 17:337–49.

Menache MG, Miller FJ, Raabe OG. 1995. Particle inhalability curves for humans and small laboratory animals. Ann Occup Hyg 39:317–28.

Nielsen GD. 1991. Mechanisms of activation of the sensory irritant receptor by airborne chemicals. Crit Rev Toxicol 21:183–208.

Pérez-Campaña C, Gomez-Vallejo V, Martin A, San SE, Moya SE, Reese T, et al. 2012. Tracing nanoparticles in vivo: a new general synthesis of positron emitting metal oxide nanoparticles by proton beam activation. Analyst 137:4902–6.

Pérez-Campaña C, Gomez-Vallejo V, Puigivila M, Martin A, Calvo-Fernandez T, Moya SE, et al. 2013. Biodistribution of different sized nanoparticles assessed by positron emission tomography: a general strategy for direct activation of metal oxide particles. ACS Nano 7:3498–505.

Sayes CM, Reed KL, Warheit DB. 2007. Assessing toxicity of fine and nanoparticles: comparing in vitro measurements to in vivo pulmonary toxicity profiles. Toxicol Sci 97:163–80.

Schleh C, Hohlfeld JM. 2009. Interaction of nanoparticles with the pulmonary surfactant system. Inhal Toxicol 21:97–103.

Taeusch HW, Bernardino de la SJ, Perez-Gil J, Alonso C, Zasadzinski JA. 2005. Inactivation of pulmonary surfactant due to serum-inhibited adsorption and reversal by hydrophilic polymers: experimental. Biophys J 89:1769–79.

Vijayaraghavan R, Schaper M, Thompson R, Stock MF, Boylstein LA, Luo JE, Alarie Y. 1994. Computer assisted recognition and quantitation of the effects of airborne chemicals acting at different areas of the respiratory tract in mice. Arch Toxicol 68:490–9.

Wang JJ, Sanderson BJ, Wang H. 2007. Cyto- and genotoxicity of ultrafine $TiO_2$ particles in cultured human lymphoblastoid cells. Mutat Res 628:99–106.

Warheit DB, Webb TR, Reed KL, Frerichs S, Sayes CM. 2007. Pulmonary toxicity study in rats with three forms of ultrafine-$TiO_2$ particles: differential responses related to surface properties. Toxicology 230:90–104.

Warheit DB, Webb TR, Sayes CM, Colvin VL, Reed KL. 2006. Pulmonary instillation studies with nanoscale TiO2 rods and dots in rats: toxicity is not dependent upon particle size and surface area. Toxicol Sci 91:227–36.

Zhang L, Yu P. 2015. Empirical equations for nasal deposition of inhaled particles in small laboratory animals and humans. Aeros Sci Technol 19:51–6.

**Supplementary material available online**